

Photoelectron ionization spectra in a system interacting with a neighbor atom

Jan Peřina Jr.,¹ Antonín Lukš,² Wiesław Leoński,³ and Vlasta Peřinová²

¹*Institute of Physics of AS CR, Joint Laboratory of Optics,
17. listopadu 50a, 772 07 Olomouc, Czech Republic*

²*Palacký University, RCPTM, Joint Laboratory of Optics,
17. listopadu 12, 771 46 Olomouc, Czech Republic*

³*Quantum Optics and Engineering Division, Institute of Physics,
University of Zielona Góra, Prof. Z. Szafrana 4a, 65-516 Zielona Góra, Poland*

Photoelectron ionization spectra of a system interacting with a neighbor two-level atom are investigated using the Laplace-transform method. These spectra are typically composed of several peaks. Photoelectron ionization spectra conditioned by the measurement on the two-level atom show oscillations at the Rabi frequency. The presence of spectral zeros occurring periodically with the Rabi period is predicted. This phenomenon is analyzed in detail.

PACS numbers: 32.80.-t,33.80.Eh,34.20.-b

I. INTRODUCTION

Ionization of an atom represents one of the most important physical effects. In this process an electron in a bound state at an atom is moved into a free state. There exist several mechanisms leading to ionization, e.g., thermal ionization or ionization in a strong static electric or magnetic field. Optical ionization is probably the most important, because it allows a versatile diagnostics of the electron system of the studied atom. At the quantum level, an electron in the bound state moves to a free state after absorbing one photon (or several photons) from the optical field. This implies that photoelectron ionization spectra depend strongly on the frequency of the optical field.

Shapes of the photoelectron ionization spectra are influenced by many factors. Among them, the presence of discrete bound excited electron states at the atom plays a dominant role as was pointed out for the first time by Fano [1]. The presence of such excited bound states thus forms additional ionization paths that compete with direct ionization. Along these additional paths, an electron moves from its ground bound state to an excited bound state due to the optical field first and, subsequently, the Coulomb configurational interaction transfers the electron into a free state. Interference among direct and indirect ionization paths determines the shapes of photoelectron ionization spectra [1–3]. Fano has shown that there exist free states that cannot be populated owing to a completely destructive interference of the ionization paths. This effect is referred to as the presence of Fano zeros that do not depend on the optical-field strength. Experimental evidence of the Fano zeros has been brought, e.g., in [4]. In general, there exist N Fano zeros in a system with N discrete levels [1]. Special attention has been devoted to auto-ionization systems with two levels in various configurations [5–8]. The interaction of auto-ionization systems with quantum optical fields has been addressed in [9]. Also the transparency for ultra-short optical pulses has been predicted in auto-ionization sys-

tems [10]. Auto-ionization systems can even slow-down the propagating light under certain conditions [11]. Similarly as other physical effects, the dynamics of ionization can be tailored using the Zeno and anti-Zeno effects [12]. Moreover, quite recently Chu and Lin [13] have proposed the method of ultra-fast Fano resonances in the description of dynamics using the model involving ultra-short laser pulses. It should be stressed out that the problem of Fano resonances is not restricted to the atomic physics only. There are numerous papers in the field of solid state physics, especially devoted to the systems containing quantum dots and nano-particles. For instance, the influence of the effect of Fano resonances on the photon statistics has been discussed in [14]. A wider overview of literature devoted to the Fano resonances in nano-physics can be found in [15].

Here, we study the role of bound excited states located at a neighbor atom in the formation of photoelectron ionization spectra [16]. An electron in a bound state of the neighbor atom interacts with an electron at the ionization atom through the dipole-dipole interaction that leads to energy transfer between two electrons [17]. This type of interaction (energy transfer) qualitatively differs from that embedded in the Fano model (electron transfer). As a consequence, the Fano zeros do not exist in this model. However, another type of spectral zeros has been discovered here and is named dynamical zeros. Such dynamical zeros occur periodically with the Rabi frequency in the conditional photoelectron ionization spectra. If bound auto-ionizing states in the ionization system are present, both the Fano and dynamical zeros can be found in photoelectron ionization spectra, as will be discussed in a consecutive publication. Suitable candidates for an experimental verification of the presented theory are molecular condensates, in which the electrons localized at different molecules interact through the dipole-dipole interaction [17]. The developed theory can also be testified using quantum dots and other semiconductor heterostructures [15].

The paper is organized as follows. In Sec. II, the model Hamiltonian is given and the corresponding dynamical

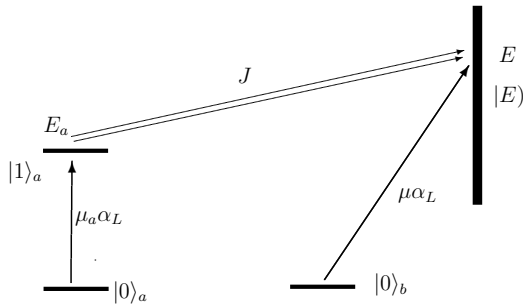


FIG. 1. Scheme of the ionization system b interacting with a two-level atom a . The state $|1\rangle_a$ refers to an excited state of atom a with the energy E_a and the symbol $|E\rangle$ denotes a free state of atom b inside the continuum with the energy E . The symbols μ_a and μ stand for the dipole moments between the ground states $|0\rangle_a$ and $|0\rangle_b$ and the corresponding excited states, respectively; α_L is the pumping amplitude. The constant J quantifies energy transfer due to the dipole-dipole interaction between the states $|1\rangle_a$ and $|E\rangle$; the double arrow indicates that two electrons at the atoms a and b participate in a given interaction.

equations are solved. Photoelectron ionization spectra in the long-time limit are studied in Sec. III. In Sec. IV, the profiles of long-time photoelectron ionization spectra are discussed and compared with those of the Fano model. The dynamical and Fano-like spectral zeros are investigated in Sec. V. Conclusions are drawn in Sec. VI.

II. QUANTUM MODEL OF THE SYSTEM AND ITS DYNAMICS

We consider an ionization system that interacts with a neighbor two-level atom by energy transfer (for the scheme, see Fig. 1). Both atoms are under the influence of a stationary optical field. The Hamiltonian \hat{H}_{ion} of ionization atom b with flat continuum levels interacting with the optical field can be written in the form ($\hbar = 1$ is assumed, [18]):

$$\hat{H}_{\text{ion}} = \int dE E |E\rangle \langle E| + \int dE [\mu \alpha_L \exp(-iE_L t) |E\rangle_b \langle 0| + \text{H.c.}]. \quad (1)$$

Here, the continuum of states of atom b is formed by the states $|E\rangle$ with the energies E . The dipole moment μ characterizes an optical excitation of the continuum states; α_L stands for an optical-field amplitude that oscillates at the frequency E_L . The symbol H.c. denotes the Hermitian conjugate term. It should be noted that the field frequency and the energies of atomic levels are chosen in such a way that the possible excitation to the continuum is located far above the ionization threshold. This assumption allows to neglect the threshold effects

and it simplifies calculations of the integrals over the continuum energies later.

The neighbor two-level atom a with its dipole moment μ_a being under the influence of the optical field is characterized by the Jaynes-Cummings Hamiltonian \hat{H}_{t-a} :

$$\hat{H}_{t-a} = E_a |1\rangle_a \langle 1| + [\mu_a \alpha_L \exp(-iE_L t) |1\rangle_a \langle 0| + \text{H.c.}]. \quad (2)$$

The state $|1\rangle_a$ refers to an excited state of atom a with the energy E_a and the ground state is denoted as $|0\rangle_a$. We note that the ground states of atoms a and b are assumed to have the same energy that is chosen to be zero.

Energy of the interaction between the two-level atom a and the ionization system b is given by the Hamiltonian \hat{H}_{trans} :

$$\hat{H}_{\text{trans}} = \int dE J |E\rangle_b \langle 0| |0\rangle_a \langle 1| + \text{H.c.} \quad (3)$$

This energy arises from the dipole-dipole interaction between two electrons at the atoms a and b [17]. Contrary to the optical dipole interaction, both electrons take part in this interaction and change their states. One electron returns from its excited state into the ground state, whereas the other one takes the left energy and moves from the ground state into its own excited state. The constant J quantifies this energy transfer between the atoms.

We assume that the electrons at both the two-level atom a and the ionization system b are initially in their ground states. The interaction of two electrons at the atoms a and b with the optical field as well as their mutual interaction lead to the evolution that can be conveniently described in the rotating frame. In this frame, a quantum state $|\psi\rangle$ can be decomposed into the following general form:

$$|\psi\rangle(t) = c_{00}(t) |0\rangle_a |0\rangle_b + c_{10}(t) |1\rangle_a |0\rangle_b + \int dE d_0(E, t) |0\rangle_a |E\rangle + \int dE d_1(E, t) |1\rangle_a |E\rangle. \quad (4)$$

The coefficients of decomposition, c_{00} , c_{10} , $d_0(E)$, and $d_1(E)$, are time dependent.

The dynamics of the composite system governed by the Schrödinger equation with the Hamiltonian $\hat{H}_{\text{ion}} + \hat{H}_{t-a} + \hat{H}_{\text{trans}}$ can be conveniently described using differential equations for the coefficients of decomposition of the state $|\psi\rangle$ in Eq. (4):

$$i \frac{d}{dt} \begin{bmatrix} \mathbf{c}(t) \\ \mathbf{d}(E, t) \end{bmatrix} = \begin{bmatrix} \mathbf{A} & \mathbf{B} \int dE \\ \mathbf{B}^\dagger & \mathbf{K}(E) \end{bmatrix} \begin{bmatrix} \mathbf{c}(t) \\ \mathbf{d}(E, t) \end{bmatrix}. \quad (5)$$

Here, the symbol \dagger means the Hermitian conjugation. In Eq. (5), the vectors \mathbf{c} and \mathbf{d} and the matrices \mathbf{A} , \mathbf{B} , and

\mathbf{K} take the form:

$$\mathbf{c}(t) = \begin{bmatrix} c_{00}(t) \\ c_{10}(t) \end{bmatrix}, \quad \mathbf{d}(E, t) = \begin{bmatrix} d_0(E, t) \\ d_1(E, t) \end{bmatrix}, \quad (6)$$

$$\mathbf{A} = \begin{bmatrix} 0 & \mu_a^* \alpha_L^* \\ \mu_a \alpha_L & \Delta E_a \end{bmatrix}, \quad (7)$$

$$\mathbf{B} = \begin{bmatrix} \mu^* \alpha_L^* & 0 \\ J^* & \mu^* \alpha_L^* \end{bmatrix}, \quad (8)$$

$$\mathbf{K}(E) = \begin{bmatrix} E - E_L & \mu_a^* \alpha_L^* \\ \mu_a \alpha_L & E - E_L + \Delta E_a \end{bmatrix}; \quad (9)$$

$\Delta E_a = E_a - E_L$. We note that the norm of state $|\psi\rangle(t)$ is conserved during the evolution, which implies the equality:

$$\sum_{j=0}^1 |c_{j0}(t)|^2 + \sum_{j=0}^1 \int dE |d_j(E, t)|^2 = 1. \quad (10)$$

The system of differential equations (5) can be analytically solved using the Laplace transform. Transforming Eqs. (5), we arrive at the following system of algebraic equations ($\varepsilon > 0$):

$$\left(\varepsilon \mathbf{1}_4 - \begin{bmatrix} \mathbf{A} & \mathbf{B} \int dE \\ \mathbf{B}^\dagger & \mathbf{K}(E) \end{bmatrix} \right) \begin{bmatrix} \tilde{\mathbf{c}}(\varepsilon) \\ \tilde{\mathbf{d}}(E, \varepsilon) \end{bmatrix} = i \begin{bmatrix} \mathbf{c}(0) \\ \mathbf{0}_2 \end{bmatrix}, \quad (11)$$

where the vector $\mathbf{c}(0) \equiv \mathbf{c}(t=0)$ describes the initial conditions. The symbol $\mathbf{1}_k$ stands for the unity matrix in k dimensions, whereas the symbol $\mathbf{0}_k$ means the zero vector with k elements.

The coefficients $\tilde{d}_0(E, \varepsilon)$ and $\tilde{d}_1(E, \varepsilon)$ describing the continuum can be determined from the last two equations in (11):

$$\tilde{\mathbf{d}}(E, \varepsilon) = [\varepsilon \mathbf{1}_2 - \mathbf{K}(E)]^{-1} \mathbf{B}^\dagger \tilde{\mathbf{c}}(\varepsilon). \quad (12)$$

The substitution of Eqs. (12) into the first two equations (11) leaves us with two equations only for the coefficients \tilde{c}_{00} and \tilde{c}_{10} :

$$\left(\varepsilon \mathbf{1}_2 - \mathbf{A} - \mathbf{B} \int dE [\varepsilon \mathbf{1}_2 - \mathbf{K}(E)]^{-1} \mathbf{B}^\dagger \right) \times \tilde{\mathbf{c}}(\varepsilon) = i \mathbf{c}(0). \quad (13)$$

The inverse matrix $[\varepsilon \mathbf{1}_2 - \mathbf{K}(E)]^{-1}$ occurring in Eq. (13) can be decomposed conveniently as follows:

$$[\varepsilon \mathbf{1}_2 - \mathbf{K}(E)]^{-1} = \sum_{k=1}^2 \mathbf{K}_k \frac{1}{E - \varepsilon - \xi_k}. \quad (14)$$

The energies ξ_1 and ξ_2 give oscillations of the two-level atom a :

$$\xi_{1,2} = E_L - \frac{\Delta E_a \pm \delta \xi}{2}, \quad \delta \xi = \sqrt{(\Delta E_a)^2 + 4|\mu_a \alpha_L|^2}. \quad (15)$$

The matrices \mathbf{K}_1 and \mathbf{K}_2 introduced in Eq. (14) have the form:

$$\mathbf{K}_k = \frac{(-1)^k}{\delta \xi} \begin{bmatrix} E_a + \xi_k & -\mu_a^* \alpha_L^* \\ -\mu_a \alpha_L & E_L + \xi_k \end{bmatrix}. \quad (16)$$

The integration of equation (14) over the energies E of continuum from $-\infty$ to ∞ provides a useful relation that considerably simplifies the system of equations (13):

$$\int dE [\varepsilon \mathbf{1}_2 - \mathbf{K}(E)]^{-1} = -i\pi \mathbf{1}_2. \quad (17)$$

Equation (13) then represents an eigenvalue problem for a newly defined matrix \mathbf{M} :

$$(\varepsilon \mathbf{1}_2 + \mathbf{M}) \tilde{\mathbf{c}}(\varepsilon) = i \mathbf{c}(0), \quad (18)$$

$$\mathbf{M} = \mathbf{A} - i\pi \mathbf{B} \mathbf{B}^\dagger. \quad (19)$$

The substitution from Eqs. (7) and (8) provides the matrix \mathbf{M} :

$$\mathbf{M} = \begin{bmatrix} -i\pi |\mu \alpha_L|^2 & M_a^c \alpha_L \\ M_a \alpha_L & \Delta E_a - i\pi (|J|^2 + |\mu \alpha_L|^2) \end{bmatrix}; \quad (20)$$

$$M_a = \mu_a - i\pi \mu J^* \text{ and } M_a^c = \mu_a^* - i\pi \mu^* J.$$

Introducing a matrix Λ_M with the eigenvalues $\Lambda_{M,j}$ on its diagonal and the matrix of eigenvectors \mathbf{P} ($\mathbf{M} = \mathbf{P} \Lambda_M \mathbf{P}^{-1}$), the solution of Eq. (18) can be written as follows:

$$\tilde{\mathbf{c}}(\varepsilon) = i \mathbf{P} \mathbf{U}_\varepsilon(\varepsilon) \mathbf{P}^{-1} \mathbf{c}(0), \quad (21)$$

where

$$[\mathbf{U}_\varepsilon]_{jk}(\varepsilon) = \frac{\delta_{jk}}{\varepsilon - \Lambda_{M,j}}. \quad (22)$$

The symbol δ_{jk} means the Kronecker δ .

The inverse Laplace transform finally gives us the temporal evolution of coefficients c_{00} and c_{10} :

$$\mathbf{c}(t) = \mathbf{P} \mathbf{U}(t) \mathbf{P}^{-1} \mathbf{c}(0) \quad (23)$$

and

$$\mathbf{U}_{jk}(t) = \delta_{jk} \exp(-i\Lambda_{M,j}t). \quad (24)$$

The substitution of the spectral solution for the coefficients $\tilde{\mathbf{c}}$ from Eq. (21) into Eq. (12) and the subsequent inverse Laplace transform leave us with the temporal coefficients $d_0(E)$ and $d_1(E)$ of the continuum:

$$\mathbf{d}(E, t) = i \sum_{k=1}^2 \mathbf{K}_k \mathbf{B}^\dagger \mathbf{P} \mathbf{U}_k(E, t) \mathbf{P}^{-1} \mathbf{c}(0); \quad (25)$$

$$[\mathbf{U}_k]_{jl}(E, t) = \frac{i\delta_{jl}}{E - \Lambda_{M,j} - \xi_k} \times [\exp[i(\xi_k - E)t] - \exp(-i\Lambda_{M,j}t)]. \quad (26)$$

If we restrict our attention to the case in which both electrons are initially in their ground states $|0\rangle_a$ and $|0\rangle_b$,

the solution written in Eq. (25) can be recast into a simplified form:

$$\mathbf{d}(E, t) = i \sum_{k=1}^2 \mathbf{D}_k \mathbf{u}_{\xi_k}(E, t), \quad (27)$$

$$[\mathbf{u}_{\xi_k}]_j(E, t) = \frac{i}{E - \Lambda_{M,j} - \xi_k} [\exp[i(\xi_k - E)t] - \exp(-i\Lambda_{M,j}t)], \quad j = 1, 2. \quad (28)$$

The eigenvalues $\Lambda_{M,j}$ of matrix \mathbf{M} can be analytically derived as follows:

$$\Lambda_{M,1,2} = \mathcal{E}_a - i\pi|\mu\alpha_L|^2 \mp \sqrt{\mathcal{E}_a^2 + M_a M_a^c |\alpha_L|^2}, \quad (29)$$

where $\mathcal{E}_a = (\Delta E_a - i\gamma_a)/2$. Moreover, the knowledge of eigenvectors of the matrix \mathbf{M} allows us to determine the matrices \mathbf{D}_1 and \mathbf{D}_2 introduced in Eq. (27). Their matrix elements give weights to the Lorentzian profiles that constitute the photoelectron ionization spectra. These matrix elements $[\mathbf{D}_k]_{jl}$ are defined along the formula $[\mathbf{D}_k]_{jl} = [\mathbf{K}_k \mathbf{B}^\dagger \mathbf{P}]_{jl} [\mathbf{P}^{-1}]_{l1}$ that provides the following explicit relations:

$$\begin{aligned} \mathbf{D}_k &= \frac{1}{\delta\xi D} \begin{bmatrix} D_{k,11} & D_{k,12} \\ D_{k,21} & D_{k,22} \end{bmatrix}; \quad (30) \\ D_{k,11} &= [\mu\tilde{\mathcal{E}}^2 + JM_a\tilde{\mathcal{E}}] \alpha_L [\pm\Delta E_a/2 + \delta\xi/2] \\ &\quad \mp \mu\mu_a^* M_a \alpha_L |\alpha_L|^2 \tilde{\mathcal{E}}, \\ D_{k,12} &= [\mu M_a M_a^c \alpha_L |\alpha_L|^2 - JM_a \alpha_L \tilde{\mathcal{E}}] \\ &\quad \times [\pm\Delta E_a/2 + \delta\xi/2] \pm \mu\mu_a^* M_a \alpha_L |\alpha_L|^2 \tilde{\mathcal{E}}, \\ D_{k,21} &= \mp \mu\mu_a \alpha_L^2 \tilde{\mathcal{E}}^2 \mp J\mu_a M_a \alpha_L^2 \tilde{\mathcal{E}} \\ &\quad + \mu M_a \alpha_L^2 \tilde{\mathcal{E}} [\mp\Delta E_a/2 + \delta\xi/2], \\ D_{k,22} &= \mp \mu\mu_a M_a M_a^c \alpha_L^2 |\alpha_L|^2 \pm J\mu_a M_a \alpha_L^2 \tilde{\mathcal{E}} \\ &\quad + \mu M_a \alpha_L^2 \tilde{\mathcal{E}} [\pm\Delta E_a/2 - \delta\xi/2], \\ \tilde{\mathcal{E}} &= -\mathcal{E}_a - \sqrt{\mathcal{E}_a^2 + M_a M_a^c |\alpha_L|^2}, \\ D &= -\tilde{\mathcal{E}}^2 - M_a M_a^c |\alpha_L|^2. \end{aligned}$$

The Rabi frequency $\delta\xi$ has been introduced in Eq. (15).

The analysis of temporal behavior of the ionization system has shown that the atom b is completely ionized for sufficiently long times. The electron from the atom b is transferred to the continuum and then left in a state that is quantum correlated (entangled) with the state of the electron at the two-level atom a . Discussion of this phenomenon will be presented elsewhere. The photoelectron ionization spectrum is composed of four Lorentzian curves as Eq. (27) indicates. Weights of these curves change in time until they reach their long-time values. We note that, in general, these weights depend also on the initial conditions for the atoms a and b . As we consider the photoelectron ionization spectra obtained in stationary optical fields, their long-time limit is of prominent interest for us.

III. LONG-TIME PHOTOELECTRON IONIZATION SPECTRA

The long-time photoelectron ionization spectral profiles are derived from the long-time form of coefficients $d_0(E, t)$ and $d_1(E, t)$ given in Eq. (25). In this limit, i.e., for the times t obeying $t \gg 1/|\text{Im}\{\Lambda_{M,j}\}|$ for $j = 1, 2$ (Im means the imaginary part), the formulas for the evolution matrices $\mathbf{U}_k(E, t)$ and vectors $\mathbf{u}_{\xi_k}(E, t)$ in Eqs. (26) and (28), respectively, considerably simplify:

$$\begin{aligned} [\mathbf{U}_k^{\text{lt}}]_{jl}(E, t) &= \delta_{jl} [\mathbf{u}_{\xi_k}]_j(E, t) \\ &= \frac{i\delta_{jl} \exp[i(\xi_k - E)t]}{E - \Lambda_{M,j} - \xi_k}; \quad (31) \end{aligned}$$

the superscript lt stands for long time. The expressions for the evolution matrices \mathbf{U}_k^{lt} in Eq. (31) show that there exist two prominent frequencies ξ_1 and ξ_2 of periodic oscillations in this long-time limit. That is why we decompose the long-time spectra \mathbf{d}^{lt} of an ionized electron at the atom b into parts \mathbf{d}^{ξ_1} and \mathbf{d}^{ξ_2} containing oscillations at the frequencies ξ_1 and ξ_2 , respectively:

$$\begin{aligned} \mathbf{d}^{\text{lt}}(E, t) &= \mathbf{d}^{\xi_1}(E, t) + \mathbf{d}^{\xi_2}(E, t), \quad (32) \\ \mathbf{d}^{\xi_i}(E, t) &= i\mathbf{K}_j \mathbf{B}^\dagger \mathbf{P} \mathbf{U}_k^{\text{lt}}(E, t) \mathbf{P}^{-1} \mathbf{c}(0), \\ &\quad j = 1, 2. \quad (33) \end{aligned}$$

The form of the amplitude long-time photoelectron ionization spectra \mathbf{d}^{lt} as written in Eq (32) means that the intensity photoelectron ionization spectra $I_j^{\text{lt}} \equiv |d_j^{\text{lt}}|^2$, $j = 0, 1$, can be decomposed into two contributions. The first steady-state contributions denoted as I_0^{st} and I_1^{st} are time independent, whereas the second ones with the common magnitude I^{osc} harmonically oscillate at the Rabi frequency $\xi_1 - \xi_2 = \delta\xi$:

$$I_j^{\text{lt}}(E, t) = I_j^{\text{st}}(E) + I_j^{\text{osc}}(E) \cos[\delta\xi t + \varphi_j(E)], \quad (34)$$

$$\varphi_j(E) = \arg[\mathbf{d}_{j+1}^{\xi_1}(E) \mathbf{d}_{j+1}^{\xi_2*}(E)],$$

$$I_j^{\text{st}}(E) = |\mathbf{d}_{j+1}^{\xi_1}(E)|^2 + |\mathbf{d}_{j+1}^{\xi_2}(E)|^2, \quad (35)$$

$$I_j^{\text{osc}}(E) = 2|\mathbf{d}_{j+1}^{\xi_1}(E)| |\mathbf{d}_{j+1}^{\xi_2}(E)|, \quad j = 0, 1. \quad (36)$$

The symbol arg denotes the argument of a complex number. It holds that $\varphi_0(E) = \varphi_1(E) \pm \pi$ and $I_0^{\text{osc}}(E) = I_1^{\text{osc}}(E) \equiv I^{\text{osc}}(E)$. Thus the overall photoelectron ionization spectrum $I^{\text{lt}}(E) = I_0^{\text{lt}}(E, t) + I_1^{\text{lt}}(E, t)$ is time independent and can be determined along the formula:

$$I^{\text{lt}}(E) = I_0^{\text{st}}(E) + I_1^{\text{st}}(E). \quad (37)$$

We note that the oscillations at the Rabi frequency $\delta\xi$ in the long-time limit can be alternatively moved into the evolution of the state of atom a provided that a suitable basis in the space of states of the ionized electron is chosen.

In order to observe temporal oscillations in a photoelectron ionization spectrum, the time-resolved spectroscopy of ionized electrons is needed. The measurement of ionization spectra has also to be done in the

post-selection regime, after the measurement whose result guarantees the presence of an electron at the atom a either in the ground state or the excited state. The temporal resolution needed depends linearly on the strength of the stationary pumping field [18]. If the experimental temporal resolution is not sufficient, just steady state parts $I_0^{\text{st}}(E)$ and $I_1^{\text{st}}(E)$ are observed.

Two prominent features may characterize the photoelectron ionization spectra in the long-time limit: the presence of the Fano and dynamical zeros.

The term Fano zero denotes a frequency in the photoelectron ionization spectrum that cannot be excited for any strength of the optical pumping. The frequency E_F of a Fano zero can thus be revealed from the condition

$$I^{\text{lt}}(E_F) = 0. \quad (38)$$

According to Eq. (37), a Fano zero at the frequency E_F occurs provided that both $I_0^{\text{st}}(E_F) = 0$ and $I_1^{\text{st}}(E_F) = 0$. In the investigated model, a genuine Fano zero does not exist, since we have not included into our model an auto-ionizing state. However, the Fano-like zeros can be observed for the case of a weak optical pumping.

The long-time photoelectron ionization spectral intensity components I_0^{st} , I_1^{st} , and I^{osc} obey in general the inequalities $I_0^{\text{st}}(E) \geq I^{\text{osc}}(E)$ and $I_1^{\text{st}}(E) \geq I^{\text{osc}}(E)$. This means that there might occur the frequencies E_D fulfilling one or both the following relations:

$$I_j^{\text{st}}(E_D) = I^{\text{osc}}(E_D), \quad j = 0, 1. \quad (39)$$

At these frequencies E_D , the long-time photoelectron ionization intensity spectrum $I_0^{\text{lt}}(E, t_D)$ [or $I_1^{\text{lt}}(E, t_D)$] equals zero at specific time instants t_D . We call these frequencies E_D dynamical zeros, because they periodically occur with the Rabi period $2\pi/\delta\xi$. They represent an analogy to the usual Fano zeros in systems that involve an additional two-level atom a oscillating in a stationary optical field. It holds that the dynamical zeros in the spectra I_0^{lt} and I_1^{lt} occur, in general, at different frequencies E_D . We will see later that the frequencies E_D of dynamical zeros in the long-time photoelectron spectra I_0^{lt} and I_1^{lt} coincide provided that the atom a is resonantly pumped.

If there exists a Fano zero at the frequency E_F , there also occurs a dynamical zero at the same frequency $E_D = E_F$. This can easily be understood from the conditions written in Eqs. (38) and (39) using the nonnegativity of intensities.

IV. DISCUSSION OF SHAPES OF LONG-TIME PHOTOELECTRON IONIZATION SPECTRA

There exists a similarity of the long-time photoelectron ionization spectra in the studied ionization system interacting with a neighbor atom and the well-known Fano model. That is why we first summarize the main features of the spectra in the Fano model and then we continue by comparing the spectra in both models.

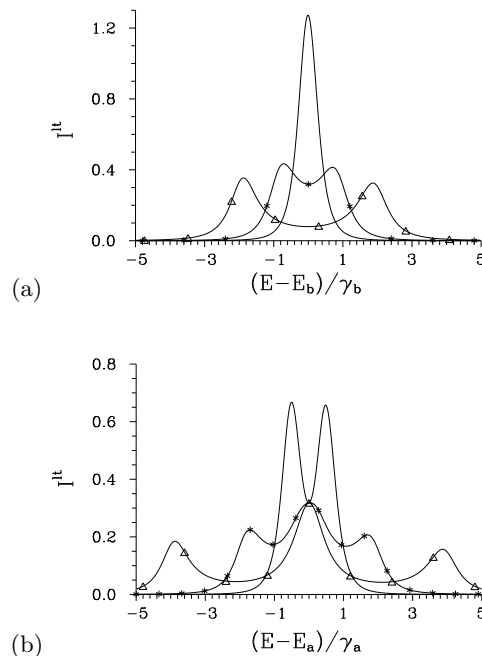


FIG. 2. Long-time photoelectron ionization spectra I^{lt} in (a) the Fano model ($q_a = \gamma_a = 0$, $q_b = 100$, $\gamma_b = 1$) and (b) the ionization system interacting with a neighbor ($q_a = 100$, $\gamma_a = 1$, $q_b = \gamma_b = 0$) in the regime of prevailing indirect ionization for several values of pumping parameter Ω : $\Omega = 1$ (solid curve), $\Omega = 2$ (solid curve with *), and $\Omega = 4$ (solid curve with \triangle); $q_a = \mu_a/(\pi\mu J^*)$, $\gamma_a = \pi|J|^2$, $q_b = \mu_b/(\pi\mu V^*)$, $\gamma_b = \pi|V|^2$, $\Omega = \sqrt{4\pi\Gamma(Q+i)\mu\alpha_L}$, $\Gamma = \gamma_a + \gamma_b$, $Q = (\gamma_a q_a + \gamma_b q_b)/\Gamma$. Spectra are normalized such that $\int dE I^{\text{lt}}(E) = 1$; $E_a = E_b = E_L = 1$.

A. Long-time photoelectron ionization spectra in the Fano model

The photoelectron ionization spectra of the usual Fano model of the atom b with one discrete excited state $|1\rangle_b$ of the energy E_b have been discussed, e.g., in [1, 2]. The state $|1\rangle_b$ can be optically excited through the dipole moment μ_b . It also interacts with the continuum of states $|E\rangle$ by the Coulomb configurational interaction that is characterized by a constant V . Thus, there occurs competition between the direct and indirect (through the state $|1\rangle_b$) ionizations. The relative strength of two ionization paths forms two distinct areas differing in shapes of the ionization spectra.

We first assume the prevailing indirect optical ionization ($q_b = \mu_b/(\pi\mu V^*) \gg 1$). In this case the long-time photoelectron ionization spectrum is peaked around the frequency E being resonant with the pumping optical frequency E_L for weaker pumping intensities [see Fig. 2(a)]. Greater pump amplitudes α_L lead to the Autler–Townes splitting [19] of this peak that results in a symmetric double-peaked spectral shape. The distance between two peaks equals $2|\mu_b\alpha_L|$. This means that the larger the pump amplitude $|\alpha_L|$, the greater the distance between two neighbor peaks. Moreover, the widths of these

peaks are proportional to $(\gamma_b + \pi|\mu\alpha_L|^2)/2$ [$\gamma_b = \pi|V|^2$], i.e., their broadening with the increasing pump amplitude α_L is observed. These conclusions can be drawn from the general form of amplitude ionization spectrum that is composed of two Lorentzian curves. These curves are centered at the frequencies $\text{Re}\{\Lambda_{M,1,2}^F\} + E_L$, where $\Lambda_{M,1,2}^F$ can be derived in the following form:

$$\begin{aligned} \Lambda_{M,1,2}^F &= \Delta E_b/2 - i\pi|\mu\alpha_L|^2/2 - i\gamma_b/2 \\ &\mp [(\Delta E_b + i\pi|\mu\alpha_L|^2 - i\gamma_b)^2 \\ &\quad + 4(\mu_b - i\pi\mu V^*)(\mu_b^* - i\pi\mu^* V)|\alpha_L|^2]^{1/2}/2; \end{aligned} \quad (40)$$

$\Delta E_b = E_b - E_L$. This formula considerably simplifies in the discussed regime if we additionally assume $\gamma_b \leq 1$ and $q_b \gg 1$:

$$\Lambda_{M,1,2}^F = \Delta E_b/2 - i\pi|\mu\alpha_L|^2/2 - i\gamma_b/2 \mp |\mu_b\alpha_L|. \quad (41)$$

On the other hand, if the direct and indirect optical ionizations are comparable, a typical shape of the photoelectron ionization spectrum consists of one peak that moves towards the lower frequencies E with the increasing pump amplitude α_L [see Fig. 3(a)]. This indicates that the Lorentzian curve centered at the frequency Λ_{M2}^F given in Eq. (40) is decisive for the spectral shape. In general, there occurs one Fano zero that originates in the destructive interference of two ionization paths. The frequency E_F of this zero is expressed as $E_F = E_b - \gamma_b q_b$.

B. Long-time photoelectron ionization spectra of an ionization system interacting with a neighbor

Now we pay attention to photoelectron ionization spectra of the ionization system interacting with a two-level neighbor atom. Here, in parallel to the direct ionization, the ionization of atom b may also occur after the energy transfer from the excited bound state $|1\rangle_a$ of atom a , that is not accompanied by the electron transfer. This indirect ionization path interferes with the path of direct ionization of the atom b . The presence of the second electron at the atom a , that undergoes the long-time stationary Rabi oscillations, substantially modifies the photoelectron ionization spectra of the Fano model discussed above. As a consequence, the photoelectron ionization spectra $d_0^{lt}(E, t)$ and $d_1^{lt}(E, t)$ belonging to the atom a in the ground and excited states, respectively, can be decomposed into two contributions oscillating at the prominent frequencies ξ_1 and ξ_2 [see Eq. (15)]. The overall photoelectron ionization spectrum I^{lt} defined in Eq. (37) is constituted by four Lorentzian curves centered around the frequencies $\text{Re}\{\Lambda_{M,j}\} + \xi_k$ for $j, k = 1, 2$ (the symbol Re denotes the real part of an argument).

As we want to compare both models at comparable conditions, we assume that the strengths of interactions leading to auto-ionization are comparable, i.e. $\gamma_a \approx \gamma_b$.

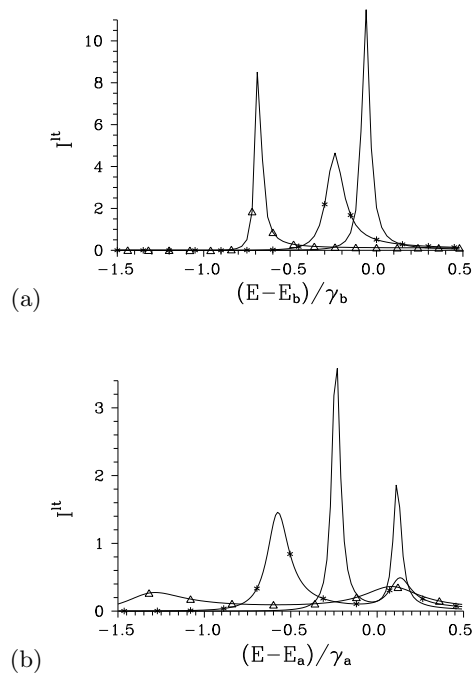


FIG. 3. Long-time photoelectron ionization spectra I^{lt} in (a) the Fano model ($q_a = \gamma_a = 0$, $q_b = \gamma_b = 1$) and (b) the ionization system interacting with a neighbor ($q_a = \gamma_a = 1$, $q_b = \gamma_b = 0$) in the regime of comparable direct and indirect ionization paths for different values of pumping parameter Ω : $\Omega = 0.5$ (solid curve), $\Omega = 1$ (solid curve with *), and $\Omega = 2$ (solid curve with Δ); $E_a = E_b = E_L = 1$.

The special case of $\gamma_a \ll \gamma_b$ appropriate for molecular condensates with their dipole-dipole and Coulomb configurational interactions is discussed at the end of Sec. IV.

Provided that the indirect ionization is much stronger than the direct one (for this case, the Fano-like asymmetry parameter $q_a = \mu_a/(\pi\mu J) \gg 1$), the assumptions of resonant pumping ($E_a = E_L$) and the weaker dipole-dipole interaction ($\gamma_a \leq 1$, $q_a \gg 1$) allows us to express four complex central frequencies in a simple form:

$$\begin{aligned} \Lambda_{M,1,2} + \xi_{1,2} &= E_L - i\gamma_a/2 - i\pi|\mu\alpha_L|^2 \\ &\mp |\mu_a\alpha_L| \mp |\mu_a\alpha_L|. \end{aligned} \quad (42)$$

These formulas indicate that the long-time photoelectron ionization spectrum consists of one central peak and two symmetric side-peaks shifted by the frequency $\pm 2|\mu_a\alpha_L|$. It can be shown that two side-peaks dominate the photoelectron spectrum for weak optical pumping, whereas three distinct peaks can be observed for stronger pumping [see Fig. 2(b)]. The widths of the spectral peaks are proportional to $\gamma_a/2 + \pi|\mu\alpha_L|^2$, i.e., the greater the pump amplitude α_L the broader the peaks. Compared to the long-time photoelectron ionization spectra of the Fano model, we additionally have the central peak and also the mutual distance of two side-peaks is twice that found in the Fano model [see Eq. (42)]. For greater pump amplitudes α_L ($\gamma_a \ll |\mu\alpha_L|^2$), the widths of the spectral peaks are twice compared to those of the Fano model.

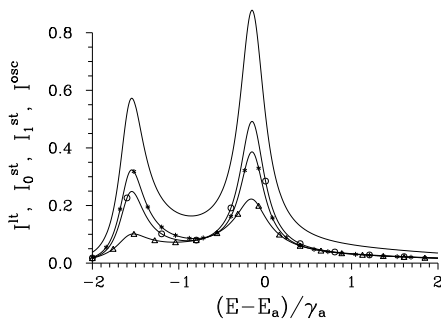


FIG. 4. Long-time photoelectron ionization spectrum I^{lt} (solid curve), its steady-state components I_0^{st} (solid curve with \circ) and I_1^{st} (solid curve with $*$), and magnitude I^{osc} of the harmonically oscillating part (solid curve with Δ) for the ionization system interacting with a neighbor under non-resonant pumping; $q_a = \gamma_a = 1$, $q_b = \gamma_b = 0$, $\Omega = 2$, $E_a = 1$, $E_L = 0.8$.

If the direct and indirect ionizations are comparable ($q_a \approx 1$), two peaks dominate the long-time photoelectron ionization spectrum, as demonstrated in Fig. 3(b). The first peak is located near the pumping frequency E_L , whereas the second one occurs around the frequency $E_L - 2|\mu_a \alpha_L|$. The second peak thus moves towards the lower frequencies when increasing the pump amplitude α_L . This behavior is qualitatively similar to that found in the Fano model [see Fig. 3(a)]. However, the frequency shift is two times larger in the ionization system interacting with a neighbor. Moreover, the spectral peaks are two times broader for stronger pumping.

Contrary to the Fano model, the long-time photoelectron spectrum I^{lt} can be decomposed into two parts I_0^{lt} and I_1^{lt} that are conditioned by the presence of the electron at the two-level neighbor atom a in the states $|0\rangle_a$ and $|1\rangle_a$, respectively. The conditional spectra I_j^{lt} are described by their steady-state components I_j^{st} and the common term I^{osc} that harmonically oscillates at the Rabi frequency $\delta\xi$. If the neighbor atom a is resonantly pumped, $I_0^{\text{st}} = I_1^{\text{st}}$. Otherwise, the two steady-state components differ in their profiles. This is illustrated in Fig. 4. For this case, two dynamical zeros around the relative frequency $(E - E_a)/\gamma_a = -0.6$ appear in the spectrum. Indeed, a closer inspection of the curves in Fig. 4 reveals that, for two frequencies in this area, the amplitude I^{osc} of the oscillating part is equal to the value of either the steady-state part I_0^{st} or the steady-state part I_1^{st} . Moreover, it should be mentioned that, the occurrence times of the two dynamical zeros in the profiles of spectra I_0^{lt} and I_1^{lt} are mutually shifted by half the Rabi period $\pi/\delta\xi$.

If molecular condensates are considered, $\gamma_a \ll \gamma_b$. In molecular condensates, the Coulomb configurational interaction constant V is typically in eV, whereas the dipole-dipole interaction (hopping) constant J is of the order of 1 – 10 meV [17]. This implies that $\gamma_a/\gamma_b \approx 10^{-4} - 10^{-6}$. Due to the scaling properties of the model the spectral profiles obtained in the regime $\gamma_a \approx \gamma_b$

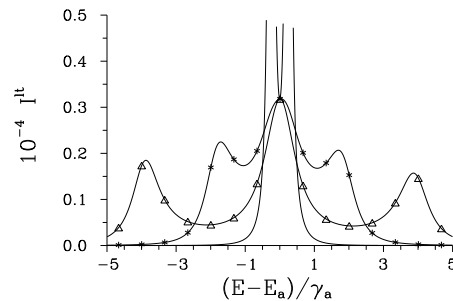


FIG. 5. Long-time photoelectron ionization spectra I^{lt} in the ionization system interacting with a neighbor for different values of pumping parameter Ω : $\Omega = 5 \times 10^{-5}$ (solid curve), $\Omega = 1 \times 10^{-4}$ (solid curve with $*$), and $\Omega = 5 \times 10^{-4}$ (solid curve with Δ); $q_a = 100$, $\gamma_a = 1 \times 10^{-4}$, $q_b = \gamma_b = 0$, $E_a = E_b = E_L = 1$.

can also be observed in this case provided that the optical pumping described by parameter Ω is weaker by four or six orders of magnitude. As an example, the long-time photoelectron ionization spectra determined for $\gamma_a = 1 \times 10^{-4}$ are shown in Fig. 5. Their profiles are similar to those valid for $\gamma_a = 1$ and drawn in Fig. 2(b). However, we should emphasize that, for $\gamma_a \ll 1$, the case of comparable dipole moments μ_a and μ of atoms a and b , respectively, is characterized by the condition $q_a \gg 1$. On the other hand, if $q_a \approx 1$ then $\mu_a \ll \mu$. Small values of dipole moments μ_a of the neighbor atom a can be reached, e.g., by the detuning of atom a from the resonance with the pumping field applying a dc electric field.

V. DYNAMICAL AND FANO-LIKE ZEROS

The frequencies of dynamical and Fano-like (for a weak optical pumping) zeros are distinguished features of the long-time photoelectron ionization spectra. We can even find them analytically in the limit of weak optical pumping ($\alpha_L \rightarrow 0$) using perturbation expansions for the matrices \mathbf{D}_j in Eq. (30) and the frequencies $\Lambda_{M,j}$ in Eq. (29) and ξ_j in Eq. (15).

A. Fano-like zeros

We first pay attention to a weak optical pumping that is in resonance with the two-level neighbor atom a ($E_a = E_L$). Under this condition, it is sufficient to express the matrices $\mathbf{D}_{1,2}$ in the first power of pump amplitude α_L and the frequencies in the zeroth power of α_L . We thus obtain:

$$\mathbf{D}_{1,2} = \left[\begin{array}{cc} -\frac{iJM_a}{\gamma_a} & -\mu + \frac{iJM_a}{\gamma_a} \\ \pm \frac{iJM_a}{\gamma_a} \frac{\mu_a}{|\mu_a|} & \pm \left(\mu - \frac{iJM_a}{\gamma_a} \right) \frac{\mu_a}{|\mu_a|} \end{array} \right] \frac{\alpha_L}{2}, \quad (43)$$

$$\Lambda_{M,1,2} + \xi_j = E_L - i\gamma_a/2 \mp i\gamma_a/2, \quad j = 1, 2. \quad (44)$$

As the rows of the matrices \mathbf{D}_1 and \mathbf{D}_2 in Eq. (43) are the same up to a multiplicative complex factor, we obtain the same equations for the frequencies of the Fano-like zeros both in the spectra d_0^{lt} and d_1^{lt} as well as in their spectral component oscillating at the frequencies ξ_1 and ξ_2 . These equations together guarantee the fulfilment of the condition for the Fano zero given in Eq. (38). They have the common form:

$$\frac{iJM_a}{\gamma_a(E_{F-l} - E_L + i\gamma_a)} + \frac{\mu - iJM_a/\gamma_a}{E_{F-l} - E_L} = 0. \quad (45)$$

The solution of Eq. (45) gives the frequency E_{F-l} of Fano-like zero at the position:

$$\frac{E_{F-l} - E_a}{\gamma_a} = -q_a; \quad (46)$$

$$q_a = \mu_a/(\pi\mu J^*).$$

In the case of weak optical pumping that is out-of-resonance with the two-level atom a ($E_a \neq E_L$), we discuss possible positions of the Fano-like zeros separately for the components oscillating at the frequencies ξ_1 and ξ_2 . As for the frequency ξ_1 , terms in the first power of α_L in the spectrum d_0^{lt} as well as terms in the third power of α_L in the spectrum d_1^{lt} lead to the same equation. We note that the restriction to the first power of α_L in the expressions for the frequencies $\Lambda_{M,j}$ and ξ_j is sufficient in this derivation. The solution of the resulting equation is independent of the detuning ΔE_a and coincides with that derived for the resonant pumping in Eq. (46).

On considering the frequency ξ_2 , the general formula for the matrices \mathbf{D}_j in Eq. (30) can be approximated by terms written in the second power of α_L both for the spectra d_0^{lt} and d_1^{lt} . These terms form two different equations for the frequencies E_{F-l} of Fano-like zeros. However, the solutions of both equations coincide and we have:

$$\frac{E_{F-l} - E_a}{\gamma_a} = -q_a - \frac{2\Delta E_a}{\gamma_a} + \frac{i\Delta E_a}{q_a\gamma_a}. \quad (47)$$

Equation (47) indicates that the non-resonant pumping of atom a moves the energy E_{F-l} of a possible Fano-like zero into the complex plane E . This means that there cannot occur any Fano-like zero in this case.

The Fano zeros in the ionization system interacting with a neighbor have been looked for numerically in the regime of stronger optical pumping. However, no Fano zero has been revealed.

B. Dynamical zeros

The frequencies E_D of dynamical zeros in the limit of weak optical pumping have been analyzed analytically in the same vein. The numerical analysis has then been found useful for arbitrarily strong pumping. The frequencies E_D of dynamical zeros are given by the general

formula in Eq. (39). Equivalently, this formula can be replaced by a more suitable one:

$$|d_j^{\xi_1}(E, t)| = |d_j^{\xi_2}(E, t)|, \quad j = 0, 1. \quad (48)$$

Similarly as in the case of Fano-like zeros, a separate discussion of the resonant and non-resonant pumping is convenient.

On assuming a weak optical pumping that is resonant with the atom a ($E_a = E_L$), the Taylor expansions of the matrices \mathbf{D}_1 and \mathbf{D}_2 in Eq. (30) to the second power of pump amplitude α_L together with the Taylor expansion of frequencies $\Lambda_{M,j}$ and ξ_j to the first power of α_L result in the following equation for the frequencies E_D :

$$\begin{aligned} & \left| \frac{JM_a - \mu\mu_a^*M_a\alpha_L/|\mu_a|}{E_D - E_a + i\gamma_a - |\mu_a\alpha_L|} \right. \\ & \quad \left. + \frac{-i\mu\gamma_a - JM_a + \mu\mu_a^*M_a\alpha_L/|\mu_a|}{E_D - E_a - |\mu_a\alpha_L|} \right| \\ & = \left| \frac{-JM_a - \mu\mu_a^*M_a\alpha_L/|\mu_a|}{E_D - E_a + i\gamma_a + |\mu_a\alpha_L|} \right. \\ & \quad \left. + \frac{i\mu\gamma_a + JM_a + \mu\mu_a^*M_a\alpha_L/|\mu_a|}{E_D - E_a + |\mu_a\alpha_L|} \right|. \end{aligned} \quad (49)$$

We note that this equation is valid for both the spectra d_0^{lt} and d_1^{lt} , i.e., the frequencies of dynamical zeros in these spectra coincide.

Equation (49) can be recast into a polynomial of the fifth order in the normalized frequency \bar{E} , $\bar{E} = (E - E_L)/\gamma_a$:

$$\begin{aligned} & |p_a|^2 \text{Im}\{p_a\}\bar{E}^5 + [-2\text{Re}\{p_a\} + \text{Im}\{p_a^2\}]\bar{E}^4 \\ & \quad + [|p_a|^2 + |p_a|^2 \text{Im}\{p_a\} - 2]\bar{E}^3 \\ & \quad + \text{Im}\{p_a^2\}\bar{E}^2 - \bar{E} = 0; \end{aligned} \quad (50)$$

$p_a = 1/q_a$. This means that up to five dynamical zeros can occur, in principle, at the same positions in the spectra I_0^{lt} and I_1^{lt} . One root of the polynomial in Eq. (50) equals zero. Provided that the parameter q_a is real, the remaining fourth-order polynomial collapses into the third-order polynomial:

$$\bar{E}^3 + \left(q_a - \frac{1}{2q_a} \right) \bar{E}^2 + \frac{q_a}{2} = 0. \quad (51)$$

The direct inspection gives one root of this polynomial at the normalized frequency $\bar{E} = -q_a$. This frequency coincides with the frequency of Fano-like zero given in Eq. (46). The remaining two roots can then be recovered easily. Thus, we arrive at the following four normalized frequencies of dynamical zeros:

$$\begin{aligned} & \frac{E_D - E_a}{\gamma_a} = 0, \\ & \frac{E_D - E_a}{\gamma_a} = -q_a, \\ & \frac{E_D - E_a}{\gamma_a} = \frac{1}{4q_a} \pm \frac{1}{4} \sqrt{\frac{1}{q_a^2} - 8}. \end{aligned} \quad (52)$$

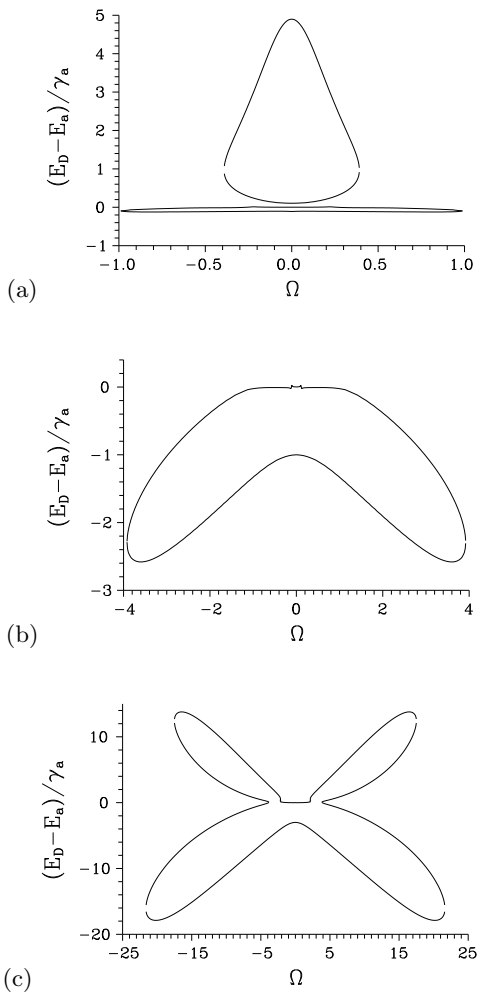


FIG. 6. Normalized frequencies $(E_D - E_a)/\gamma_a$ of dynamical zeros as they depend on pumping parameter Ω for different values of parameter q_a : (a) $q_a = 0.1$, (b) $q_a = 1$, and (c) $q_a = 3$; $\gamma_a = 1$, $q_b = \gamma_b = 0$, $E_a = E_L = 1$.

The last two normalized frequencies written in Eq. (52) are real provided that $|q_a| \leq 1/(2\sqrt{2})$.

In the case of arbitrarily strong optical pumping, up to five dynamical zeros can be discovered. They usually occur in pairs. When studying the dependence of frequencies E_D on the pumping strength Ω (for the definition, see the caption to Fig. 2, $\Omega \propto \alpha_L$), the creation and annihilation of frequency pairs has been observed (see Fig. 6). We have found three qualitatively different shapes of curves in graphs showing the dependence of normalized frequencies $(E_D - E_a)/\gamma_a$ on the pumping parameter Ω depending on the relative strengths of direct and indirect ionization paths. They are plotted in Fig. 6. In Fig. 6, the values of the frequencies E_D for $\Omega \rightarrow 0$ coincide with those analytically described in Eq. (52). We also note that the graphs in Fig. 6 are symmetric with respect to the exchange Ω by $-\Omega$.

On considering the non-resonant pumping of atom a ($E_a \neq E_L$), the frequencies E_D of dynamical zeros, in

general, differ for the photoelectron ionization spectra I_0^{lt} and I_1^{lt} . On assuming a weak optical pumping α_L and the spectrum I_0^{lt} , the Taylor expansion of the matrices \mathbf{D}_j , $j = 1, 2$, in Eq. (30) up to the first power in α_L is sufficient. The condition for dynamical zeros in Eq. (48) then reveals two normalized frequencies $(E_D - E_a)/\gamma_a$:

$$\begin{aligned} \frac{E_D - E_a}{\gamma_a} &= -q_a, \\ \frac{E_D - E_a}{\gamma_a} &= -2 \frac{\Delta E_a}{\gamma_a}. \end{aligned} \quad (53)$$

On the other hand, the Taylor expansion of matrices \mathbf{D}_j , $j = 1, 2$, up to the second power in α_L is needed when studying the frequencies E_D in the photoelectron ionization spectrum I_1^{lt} . The condition for dynamical zeros written in Eq. (48) can be recast into a fifth-order polynomial in the frequencies E_D . On assuming the real parameter q_a , this polynomial reduces to the fourth-order polynomial in the normalized frequency $\bar{E} = (E_D - E_L)/\gamma_a$:

$$\begin{aligned} &\left[4q_a + \frac{1}{q_a^2}\delta E_a\right] \bar{E}^4 + \left[-2 + 4q_a^2 + \frac{2}{q_a^2}\delta E_a^2\right] \bar{E}^3 \\ &- \left[\left(3 + \frac{1}{q_a^2}\right)\delta E_a + 4q_a\delta E_a^2 + \frac{1}{q_a^2}\delta E_a^3\right] \bar{E}^2 \\ &+ [2q_a^2 - 2q_a\delta E_a] \bar{E} + [q_a^2\delta E_a - 2q_a\delta E_a^2 + \delta E_a^3] = 0, \end{aligned} \quad (54)$$

where $\delta E_a = \Delta E_a/\gamma_a$. We note that $\Delta E_a \neq 0$ was assumed in the derivation of Eq. (54). There exist, in general, four roots of this polynomial that can be found numerically. As only real roots give the frequencies E_D , there might occur 0, 2, or 4 frequencies E_D determining positions of dynamical zeros.

Typical behavior of the dynamical zeros for the non-resonant pumping of atom a considered as a function of the pumping parameter Ω is shown in Fig. 7 for $q_a = 1$. The comparison with the graph in Fig. 6(b) reveals two characteristic features caused by the non-resonant pumping. First, the curves observed for the resonant pumping are split into two adjacent ones: one belongs to the normalized frequencies of dynamical zeros in the spectra I_0^{lt} , one gives the normalized frequencies in the spectra I_1^{lt} . Second, there occur new curves with shapes depending qualitatively on the sign of the detuning ΔE_a . The symmetry $\Omega \leftrightarrow -\Omega$ is also preserved.

We would like to emphasize a prominent role of parameter γ_a in the determination of frequencies E_D of the dynamical zeros. The parameter γ_a giving the strength of 'non-optical' auto-ionization interaction (e.g., dipole-dipole interaction) occurs in the calculations only as a scaling parameter of the frequency difference $E_D - E_a$. This means that the obtained results are applicable, after appropriate rescaling, also to the case of molecular condensates in which the dipole-dipole interaction gives $\gamma_a \approx 10^{-4} - 10^{-6}$.

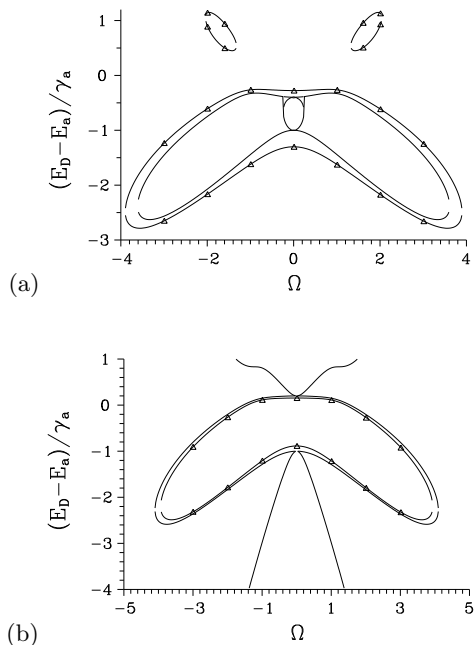


FIG. 7. Normalized frequencies $(E_D - E_a)/\gamma_a$ of dynamical zeros as they depend on pumping parameter Ω for the non-resonant pumping of atom a : (a) $E_L = 0.8$ and (b) $E_L = 1.1$. Solid curves indicate the frequencies found in the spectra I_0^{lt} , solid curves with \triangle correspond to the spectra I_1^{lt} ; $q_a = \gamma_a = 1$, $q_b = \gamma_b = 0$, $E_a = 1$.

VI. CONCLUSIONS

The long-time photoelectron ionization spectra of an ionization system interacting with a neighbor two-level

atom have been investigated using the Laplace-transform method. They have been compared with the spectra characterizing the Fano model of auto-ionization. The spectra are typically composed of several peaks of different widths depending on the pump-field intensity. As a consequence of the interference of two ionization paths, zeros in the long-time photoelectron ionization spectra may occur. Whereas the genuine Fano zeros cannot be found in this model, the Fano-like zeros occurring for a weak optical pumping can be observed. The long-time photoelectron ionization spectra conditioned by the presence of the neighbor two-level atom in a given state exhibit the permanent Rabi oscillations. Dynamical spectral zeros observed once in the Rabi period have been discovered in these conditional spectra. The frequencies of dynamical zeros depend on the strength of optical pumping as well as on the projected state of the two-level atom. The numbers as well as the values of frequencies of the dynamical zeros have been analyzed in detail. Molecular condensates have been shown to be suitable candidates for the experimental verification of the predicted effect.

ACKNOWLEDGMENTS

Support by the projects 1M06002, COST OC 09026, and Operational Program Research and Development for Innovations - European Social Fund (project CZ.1.05/2.1.00/03.0058) of the Ministry of Education of the Czech Republic as well as the project IAA100100713 of GA AV ČR is acknowledged.

-
- [1] U. Fano, Phys. Rev. **124**, 1866 (1961).
 - [2] K. Rzażewski and J. H. Eberly, Phys. Rev. Lett. **47**, 408 (1981).
 - [3] P. Lambropoulos and P. Zoller, Phys. Rev. A **24**, 379 (1981).
 - [4] L. Journel, B. Rouvellou, D. Cubaynes, J. M. Bizau, F. J. Willeumier, M. Richter, P. Sladeczek, K.-H. Selbman, P. Zimmerman, and H. Bergerow, J. de Physique IV **3**, 217 (1993).
 - [5] W. Leoński, R. Tanaś, and S. Kielich, J. Opt. Soc. Am. B **4**, 72 (1987).
 - [6] W. Leoński and R. Tanaś, J. Phys. B: At. Mol. Opt. Phys. **21**, 2835 (1988).
 - [7] W. Leoński, R. Tanaś, and S. Kielich, J. Phys. D: Appl. Phys. **21**, S125 (1988).
 - [8] W. Leoński and R. Tanaś, J. Opt. Soc. Am. B **8**, 6 (1991).
 - [9] W. Leoński and V. Bužek, J. Mod. Opt. **37**, 1923 (1990).
 - [10] E. Paspalakis, N. J. Kylstra, and P. L. Knight, Phys. Rev. A **60**, 642 (1999).
 - [11] A. Raczyński, M. Rzepecka, J. Zaremba, and S. Zielińska-Kaniasty, Optics Communications **266**, 552 (2006).
 - [12] M. Lewenstein and K. Rzażewski, Phys. Rev. A **61**, 022105 (2000).
 - [13] W.-C. Chu and C. D. Lin, Phys. Rev. A **82**, 053415 (2010).
 - [14] A. Ridolfo, O. Di Stefano, N. Fina, R. Saija, and S. Savasta, Phys. Rev. Lett. **105**, 263601 (2010).
 - [15] A. E. Miroshnichenko, S. Flach, and Y. S. Kivshar, Rev. Mod. Phys. **82**, 2257 (2010).
 - [16] A. Lukš, V. Peřinová, J. Peřina Jr., J. Křepelka, and W. Leoński, in *Wave and Quantum Aspects of Contemporary Optics: Proceedings of SPIE, Vol. 7746*, edited by J. Müllerová, D. Senderáková, and S. Jurecka (SPIE, Bellingham, 2010), p. 77460W.
 - [17] E. A. Silinsh and V. Čápek, *Organic Molecular Crystals: Interaction, Localization and Transport Phenomena* (Oxford University Press/American Institute of Physics, 1994).
 - [18] P. Meystre and P. Sargent III, *Elements of Quantum Optics* (Springer, Berlin, 2007).
 - [19] S. H. Autler and C. H. Townes, Phys. Rev. **100**, 703 (1955).